Effects of growth temperature and thermal annealing on optical quality of GaNAs nanowires emitting in the near-infrared spectral range

OPEN ACCESS
IOP Publishing
Nanotechnology

Nanotechnology **31** (2020) 065702 (6pp)
https://doi.org/10.1088/1361-6528/ab51cd

Effects of growth temperature and thermal annealing on optical quality of GaNAs nanowires emitting in the near-infrared spectral range

J E Stehr[1,3], R M Balagula[1], M Jansson[1], M Yukimune[2], R Fujiwara[2], F Ishikawa[2], W M Chen[1] and I A Buyanova[1,3]

[1] Department of Physics, Chemistry and Biology, Linköping University, SE-581 83 Linköping, Sweden
[2] Graduate School of Science and Engineering, Ehime University, 790-8577 Matsuyama, Japan

E-mail: jan.eric.stehr@liu.se and irina.bouianova@liu.se

Received 3 June 2019, revised 11 September 2019
Accepted for publication 28 October 2019
Published 13 November 2019

Abstract

We report on optimization of growth conditions of GaAs/GaNAs/GaAs core/shell/shell nanowire (NW) structures emitting at ~1 μm, aiming to increase their light emitting efficiency. A slight change in growth temperature is found to critically affect optical quality of the active GaNAs shell and is shown to result from suppressed formation of non-radiative recombination (NRR) centers under the optimum growth temperature. By employing the optically detected magnetic resonance spectroscopy, we identify gallium vacancies and gallium interstitials as being among the dominant NRR defects. The radiative efficiency of the NWs can be further improved by post-growth annealing at 680 °C, which removes the gallium interstitials.

Supplementary material for this article is available online

Keywords: GaNAs, optically detected magnetic resonance, nanowires

(Some figures may appear in colour only in the online journal)

1. Introduction

Semiconductor nanowires are considered as versatile and functional building blocks for future nano-optoelectronic and nano-electronic devices due to their unique physical properties [1–7]. Particularly, ternary group-III–V nanowires (NWs) have attracted an increasing interest due to the possibility to change their bandgap to desired energies by varying alloy compositions [7–14]. Here, Ga(In)NAs nanowires are particularly appealing [15] due to their tunable bandgap ranging from the near-infrared to infrared spectral region, which makes them an ideal material system for applications in numerous optoelectronic devices, such as light-emitting diodes and nano-lasers [16, 17]. Such bandgap tunability can be realized by minor changes in the N composition [N], facilitated by the giant bowing in the bandgap energy characteristic for these dilute nitrides [18–22]. For example, by increasing [N] from 0% to 5%, the bandgap of GaN_xAs_{1-x} can be lowered by 0.5 eV [20], i.e. towards the near-infrared spectral range important for fiber-optic communications.

Due to the large miscibility gap between nitrides and arsenides and low equilibrium solubility of N in bulk Ga(In)As [23, 24], growth of the resulting dilute nitrides is known to be challenging. Previous studies of the growth of GaNAs epilayers have demonstrated that, in order to incorporate N in GaAs while avoiding phase separation, the growth needs to be performed at rather low temperatures [18–21]. This, however,

[3] Authors to whom any correspondence should be addressed.

leads to deterioration of optical quality of the forming alloy due to increasing non-radiative recombination (NRR) via point defects [25–29]. This sets strict requirements on the growth temperature, which were found to be specific for the utilized growth methods and alloy compositions [30–34]. For example, in the case of GaInNAs epilayers Kondow *et al* [31] concluded that the optimum growth temperature is around 460 °C, whereas it was found [30] to be much higher, around 580 °C, for the GaNAs epilayers. It was also shown that the optical quality of the epilayers can be improved without sacrificing their structural quality by post-growth annealing [26, 27, 35–37]. As to GaNAs-based NWs, effects of growth temperature and post-growth annealing on their structural and optical quality are not known and will be addressed in this paper by employing photoluminescence (PL) and optically detected magnetic resonance (ODMR) spectroscopies.

2. Experimental details

The studied $GaAs/GaN_{0.02}As_{0.98}/GaAs$ core/shell/shell NWs, to be referred to as GaNAs NWs below for simplicity, were grown by Ga-catalyzed molecular beam epitaxy (MBE) on (111) Si substrates using nitrogen plasma as a nitrogen source. The NW core was formed by vapor–liquid–solid growth assisted by constituent Ga seed particles when Ga and As flux were supplied on the Si substrate. The beam equivalent pressure (BEP) of As was adjusted to 4×10^{-3} Pa throughout the growth. The Ga supply was set to match a planar growth rate of 1 ML s^{-1} for the core and 0.5 ML s^{-1} for the shell layers on GaAs (001). The V/III BEP ratio was 37 during the growth of the GaAs core. By introducing a growth interruption, the catalyst Ga became crystallized. The Ga flux was reduced to 0.5 ML during the crystallization. Subsequently, the lateral growth became dominant, enabling the formation of the GaAs/GaNAs/GaAs core-multishell structure. In order to optimize the wire nucleation, nitrogen incorporation, and crystal and optical quality, two sets of GaNAs NWs were grown under the identical growth conditions except for the growth temperature T_g. In the first set the GaAs cores were grown at 610 °C whereas T_g for the GaAs/GaNAs multishell layers was reduced to 520 °C. We will refer to this structure as high-temperature (HT) GaNAs NWs. For the second set (to be referred to as low-temperature (LT) GaNAs NWs), the growth temperature was lowered down to 580 °C and 500 °C for the GaAs core and GaAs/GaNAs multishell layers, respectively. In both structures, the N composition in the GaNAs shell was about 2%, i.e. represents the highest N concentration achievable so far for the NW structures with the high optical quality [38]. The N composition was estimated using the band anticrossing model [15, 22] from the peak position of the free exciton/carrier emission, based on temperature-dependent PL measurements. As a reference, we also investigated pure GaAs NWs grown under the identical conditions as the LT-GaNAs NWs but without igniting the nitrogen plasma. A more detailed description of the growth process can be found in [38]. After the growth, some of the samples were annealed in the MBE chamber under As_2 overpressure. The annealing was performed for 15 min at 680 °C. Representative scanning electron microscopy (SEM) images of the so-obtained as-grown NW arrays are shown in figures 1(a)–(c). Independent of T_g, all NWs are found to be uniform in size and have a length of 3–5 μm and a diameter of about 350 nm. They exhibit a hexagonal shape in cross section, which indicates that they were epitaxially grown following the Si [111] crystal orientation. Seen from figure 1, some of the NWs are randomly tilted from the [111] direction by up to 60°, which has implications on the analysis of the spin-resonance signals as will be discussed below. Figures 1(d)–(f) features SEM images of the annealed samples. Structurally, the annealed NW arrays have similar morphology as the as-grown structures though NW surface has deteriorated.

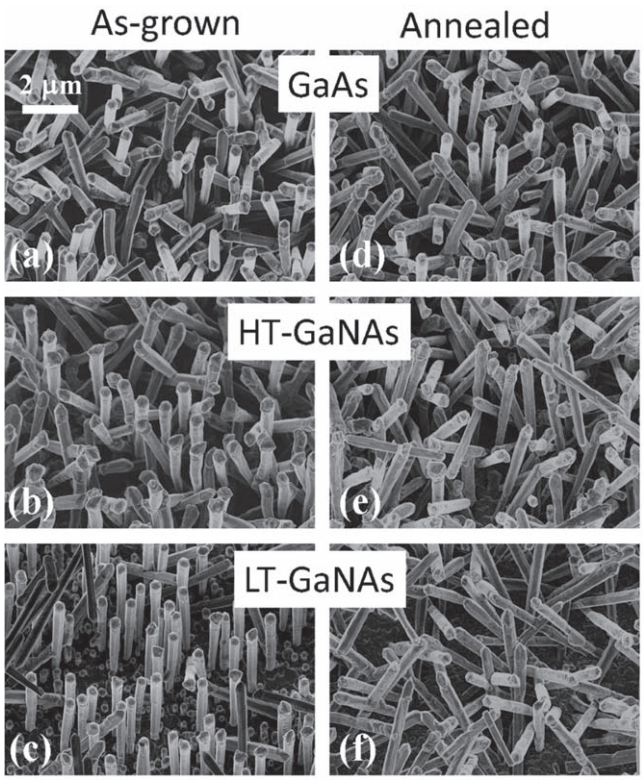

Figure 1. Representative SEM images of the as-grown GaAs NWs (a), the HT-GaNAs NWs (b) and the LT-GaNAs NWs (c). (d)–(f) are SEM images of the same structures after post-growth annealing.

Micro-PL (μ-PL) measurements were performed on the NW arrays in a variable-temperature He-flow cryostat. The samples were excited in a backscattering geometry with the 660 nm line of a solid-state laser focused to a spot of approximately 1 μm in diameter using a 50× optical objective with a numerical aperture of 0.5. The collected PL signal was detected using a grating monochromator coupled with a liquid nitrogen-cooled linear array InGaAs photodetector. A schematic drawing of the μ-PL setup is depicted in figure S1 of the supplementary material and available online at stacks.iop.org/NANO/31/065702/mmedia. ODMR measurements were conducted at 4 K at a microwave frequency of ~34 GHz (Q-band) with adjustable MW powers. ODMR signals were measured as microwave-induced changes of the PL intensity

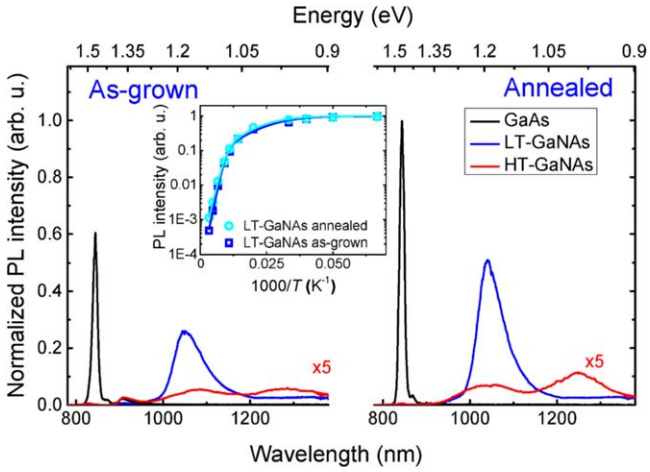

Figure 2. PL spectra from the as-grown (the left panel) and annealed (the right panel) GaAs (the black curve), HT-GaNAs (the red curve) and LT-GaNAs (the blue curve) NWs measured at 6 K. The inset displays Arrhenius plots of the integrated PL intensity (open symbols) for the as-grown and annealed LT-GaNAs NWs. The solid lines in the inset represent the best fit to the experimental data using equation (1).

excited using the 532 nm line of a solid-state laser as an excitation source and detected by a Ge detector. A schematic drawing of the ODMR setup is shown in figure S2 of the supplementary material.

3. Results and discussion

Figure 2 summarizes results of μ-PL measurements performed at 6 K on the as-grown and annealed NW arrays. The PL spectrum of the as-grown GaAs NWs contains a PL band centered at 1.47 eV, typical for zinc-blende GaAs NWs with a large degree of twinning and wurtzite WZ inclusions [39–44]. The emission shifts to lower energies in the GaNAs NWs, which suggests that the optically active region in these structures is the GaNAs shell with a lower bandgap. Changes in the growth temperature have a profound effect on the PL spectra of the GaNAs NWs. The HT-GaNAs structures demonstrate a weak near-band-edge emission at 1.15 eV overlapping with a broad defect-related PL band of a similar intensity. The intensity of the near-band-edge emission is dramatically enhanced, by about 25 times, in the LT-grown structures. This is accompanied by a small blue shift of the emission to 1.18 eV and a decrease in its linewidth. According to the previous studies, the near-band-edge emission in GaNAs alloys observed at low measurement temperatures is due to radiative recombination of excitons localized at band tail states caused by alloy fluctuations [45]. Therefore, the decrease in the PL linewidth likely reflects a decrease in the localization potential and, hence, better alloy uniformity of the GaNAs shell under the LT growth. The increase of the PL intensity in these structures implies the reduced NRR. Both of these findings clearly demonstrate that the optical quality of the LT-GaNAs NWs is superior to the HT-grown structures. We note that this behavior is opposite to that reported previously for epitaxial GaNAs [30]. Radiative efficiency of all structures can be improved by post-growth annealing—see figure 1. For example, the near-band-edge emission increases by approximately two times in the LT-GaNAs NWs, which suggests a reduction in the concentrations of the NRR defects. Its spectral position, however, is not affected by the annealing, which means that the GaNAs alloy remains chemically stable under the utilized conditions and no out-diffusion of N from the GaNAs shell occurs.

To further evaluate the role of the NRR defects, we have performed temperature-dependent PL measurements on the optimized LT-GaNAs NWs. In the inset of figure 2, we show Arrhenius plots of the integrated PL intensity measured from the as-grown and annealed structures. Despite of the growth optimization, we still observe strong thermal quenching of the PL intensity with increasing temperature (T), which becomes somewhat suppressed after annealing. The obtained dependences can be fitted using the following bi-exponential function

$$I(T) = \frac{I_0}{1 + C_1 \exp\left(-\frac{E_1}{k_B T}\right) + C_2 \exp\left(-\frac{E_2}{k_B T}\right)}. \quad (1)$$

Here $I(T)$ is the PL intensity at a given temperature T, I_0 is the PL intensity at 4 K, k_B is the Boltzmann constant, E_1 and E_2 are the activation energies for the two thermally activated processes, C_1 and C_2 are the weighing coefficients for these processes. The best fit to the experimental data before and after annealing is achieved assuming the same energies $E_1 = 12$ meV and $E_2 = 63$ meV and with almost no change in C_1 with annealing. At the same time the weighing coefficient C_2 for the dominant thermally activated process decreases by 40% after annealing (from 16 500 to 9700), which reflects the annealing-induced decrease in the number of the NRR defects responsible for the thermal quenching of the PL intensity.

To identify the defect origin, we performed detailed ODMR experiments, since the ODMR spectroscopy is capable of revealing chemical identity of a defect involved in the monitored recombination process based on resolved hyperfine interactions of defect electrons with their own nuclear core and/or the nuclei of neighboring atoms [46]. Figure 3 depicts typical ODMR spectra (the solid curves) of the investigated GaAs, HT-GaNAs and LT-GaNAs NWs obtained by monitoring the PL emissions shown in figure 2. The GaAs NWs exhibit a rather broad ODMR signal with a linewidth of approximately 100 mT, whereas ODMR spectra of the GaNAs NWs contain several overlapping peaks. To analyze the ODMR spectra and identify the involved defects, we used the following spin-Hamiltonian:

$$\mathcal{H} = \mu_B \boldsymbol{BgS} + \boldsymbol{SAI}. \quad (2)$$

It consists of two terms: (1) the Zeeman interaction term with the Bohr magneton μ_B, an external magnetic field **B**, the effective electron spin operator **S**, and the electron g-tensor **g**. (2) The hyperfine interaction term, with the nuclear spin operator **I** and the hyperfine tensor **A**. Modeling of the ODMR spectra was performed using the Easyspin software

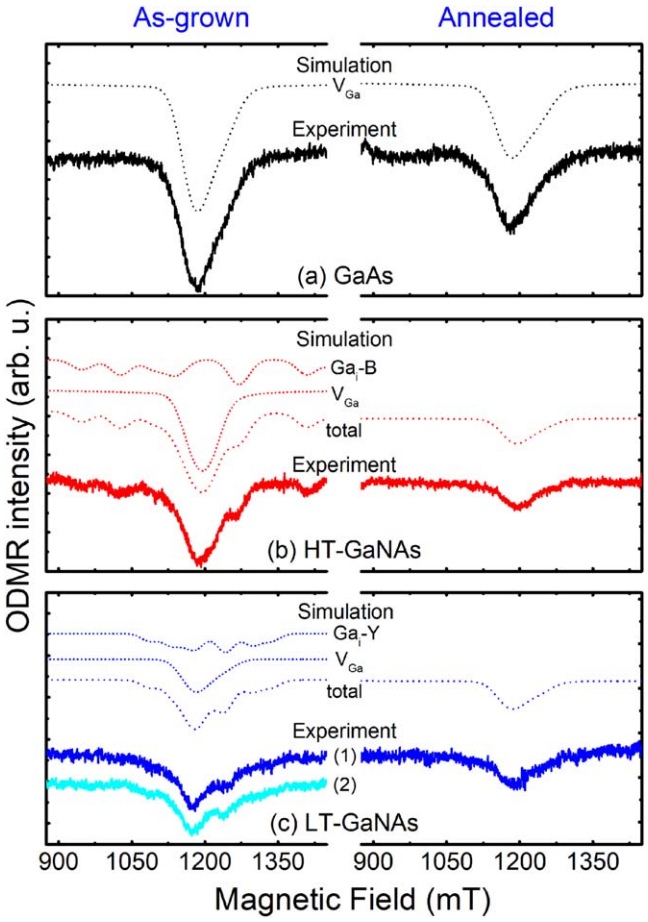

Figure 3. ODMR spectra from the GaAs (a), the HT-GaNAs (b) and the LT-GaNAs (c) NWs, measured under photo-excitation at 2.33 eV (above the GaAs bandgap). The left and right panel in (a)–(c) correspond to the results from the as-grown and annealed NWs, respectively. The solid curves represent the experimental data, while the dotted lines are simulated spectra of different defects using equation (2) and the spin-Hamiltonian parameters given in the text. The dashed lines labeled as 'total' represent the simulated spectra that include contributions from all defects. The ODMR spectrum from the as-grown LT-GaNAs NWs measured under photo-excitation of 1.4 eV is shown by the curve (2) in figure 3(c).

package [47] and taking into account random orientations of some of the NWs with tilting angles up to 60° from the vertical [111] direction, as revealed by SEM (see figure 1). This was done by averaging the ODMR spectra over all orientations corresponding to the orientation of the NWs, which caused an overall broadening and merging of anisotropic ODMR signals. Isotropic ODMR signals were of course not affected by this. The simulated ODMR spectra of the revealed defects are depicted by the dotted lines in figure 3, whereas the dashed lines labeled as 'total' represent the simulated spectra that include contributions from all defects.

The ODMR signal in the GaAs NWs (figure 3(a)) can be simulated assuming the following spin Hamiltonian parameters: $S = 1/2$, $I = 3/2$, $g_{||} = 1.98$, $g_{\perp}$=2.08, $A_{||} = 722$ MHz and $A_{\perp} = 335$ MHz. (The orientations marked as parallel and perpendicular are with respect to the crystallographic [111] axis). From these spin-Hamiltonian parameters the ODMR signal can be assigned to a gallium vacancy (V_{Ga}) with a hyperfine interaction of an unpaired electron spin $S = 1/2$ and an ^{75}As nucleus (100% natural abundance) with a nuclear spin $I = 3/2$. This defect was also observed previously in electron irradiated GaAs bulk crystals [48] and GaNAs NWs with low N compositions below 0.6% [49].

The ODMR spectrum of the HT-GaNAs NWs sample (figure 3(b)) consists of two overlapping signals. The first one is again the V_{Ga} signal, while the second one has several peaks and involves a gallium interstitial (Ga_i) atom based on the resolved hyperfine structure with two groups of four lines each (due to a nuclear spin $I = 3/2$) with a characteristic ratio of 60%–40% related to the natural abundance of the ^{69}Ga (60.1% natural abundance) and ^{71}Ga (39.9% natural abundance). The spectrum of this particular Ga_i can be fitted by using the following spin-Hamiltonian parameters: $S = 1/2$, $I = 3/2$, $g = 2.0$, $A(^{69}\text{Ga}) = 3430$ MHz and $A(^{71}\text{Ga}) = 4440$ MHz. These parameters are similar to those reported for Ga_i-B in GaNAs thin-films [50].

In the ODMR spectrum of the LT-GaNAs NWs (the curve 1 in figure 3(c)), one can again detect the V_{Ga} signal. The spectrum also contains a Ga_i-related signal, which has, however, a different set of spin-Hamiltonian parameters: $S = 1/2$, $I = 3/2$, $g = 2.0$, $A(^{69}\text{Ga}) = 1550$ MHz and $A(^{71}\text{Ga}) = 2330$ MHz. These parameters are different from the spin Hamiltonian parameters of other Ga_i-related defects reported in the literature [29] and we label this new defect as Ga_i-Y. This indicates that the growth conditions have a strong influence on the formation of Ga_i-related defects in GaNAs NWs. Optical excitation by 2.33 eV photons utilized during the ODMR measurements creates non-equilibrium carriers in all spatial regions of the core/multishell NW structure, including the GaAs core and the outer-shell layer as well as the active GaNAs inner-shell. In order to single out the exact spatial location of the revealed defects within the structure, we have also measured ODMR spectra under the optical excitation with photon energy of 1.4 eV that is below the GaAs bandgap. Within the experimental error, the spectrum (the curve (2) in figure 3(c)) is found to be identical to the one measured under the excitation with energies above the GaAs bandgap (the curve (1) in figure 3(c)), proving that the majority of the defects are located in the optically-active GaNAs inner shell.

All of the detected ODMR signals are negative in sign, which means that they correspond to a microwave-induced decrease in the PL intensity and that the revealed defects act as NRR centers competing with the monitored PL. A comparison between the ODMR signal intensities between the HT-GaNAs NWs and the LT-GaNAs NWs shows that decreasing T_g leads to a decreased formation of the NRR centers which in turn results in the observed increase of the PL intensity. This behavior is opposite to that reported previously in GaNAs epilayers [30] suggesting that the defect formation is critically affected by the growth process. In all structures, post-growth thermal annealing leads to a significant decrease of the V_{Ga} ODMR intensity. Furthermore, the observed disappearance of the Ga_i-related ODMR signals in the GaNAs NWs after annealing, see figures 3(b), (c),

indicates that both types of the Ga_i-related defects can be annealed out at 680 °C. The decrease in the ODMR signal intensity qualitatively correlates with an increase of the PL intensities after annealing, confirming that the revealed NRR centers limit radiative recombination. We note that the improvement of the PL intensity after annealing may be restricted, at least to some extent, by deteriorating surface conditions, which will likely enhance surface recombination.

4. Conclusions

In summary, we have identified optimal conditions of growth temperature and post-growth thermal annealing for the GaAs/GaNAs/GaAs core–shell–shell NWs with superior optical quality owing to suppression of NRR. Ga interstitials and gallium vacancies have been found to be the dominant NRR centers in the as-grown NWs. In addition, we show that the structure of the formed Ga_i-related defects depends on the growth conditions and that a new type of Ga_i defects can be formed during the NW growth. The Ga_i-related defects are found to be thermally unstable and can be annealed out at 680 °C. The overall decrease in the number of non-radiative defects after annealing is found to result in an increase in the PL intensity and less pronounced PL thermal quenching. Such improvements are, however, likely undermined by the deterioration of the NW surface, which calls for future research effort in improving the optical quality by simultaneously suppressing the harmful NRR via both point defects and surface states.

Acknowledgments

The authors would like to acknowledge the financial support from the Swedish Energy Agency (Grant No. P40119-1), the Swedish Research Council (Grant No. 2015-05532) and the Swedish Foundation for International Cooperation in Research and Higher Education (STINT) (Grant No. JA2014-5698). IB and WMC acknowledge financial support from the Swedish Government Strategic Research Area in Materials Science on Functional Materials at Linköping University (Faculty Grant SFO-Mat-LiU No 2009 00971). The NW growth was partly supported by KAKENHI (No. 16H05970 and 23686004) from the Japan Society for the Promotion of Science, research scholarships from the Kato Foundation for Promotion of Science, the Kurata Memorial Hitachi Science and Technology Foundation, and the Murata Science Foundation.

Notes

JES and RMB contributed equally to this work.

ORCID iDs

J E Stehr https://orcid.org/0000-0001-7640-8086
R M Balagula https://orcid.org/0000-0003-0424-8516
M Jansson https://orcid.org/0000-0001-5751-6225
F Ishikawa https://orcid.org/0000-0002-5632-056X
W M Chen https://orcid.org/0000-0002-6405-9509
I A Buyanova https://orcid.org/0000-0001-7155-7103

References

[1] Joyce H J *et al* 2011 *Prog. Quantum Electron.* **35** 23
[2] Thelander C *et al* 2006 *Mater. Today* **9** 28
[3] Li Y, Qian F, Xiang J and Lieber C M 2006 *Mater. Today* **9** 18
[4] Yan R X, Gargas D and Yang P D 2009 *Nat. Photon.* **3** 569
[5] Miao J *et al* 2014 *ACS Nano* **8** 3628
[6] Ren P, Xu J, Wang Y, Zhuang X, Zhang Q, Zhou H, Wan Q, Shan Z, Zhu X and Pan A 2013 *Phys. Status Solidi Appl. Mater. Sci.* **210** 1898
[7] Ren P *et al* 2014 *Nano-Micro Lett.* **6** 301
[8] Stettner T *et al* 2018 *Nano Lett.* **18** 6292
[9] Takiguchi M, Yokoo A, Nozaki K, Birowosuto M D, Tateno K, Zhang G, Kuramochi E, Shinya A and Notomi M 2017 *APL Photonics* **2** 046106
[10] Wu Z H, Sun M, Mei X Y and Ruda H E 2004 *Appl. Phys. Lett.* **85** 657
[11] Shin J C, Kim K H, Yu K J, Hu H, Yin L, Ning C-Z, Rogers J A, Zuo J-M and Li X 2011 *Nano Lett.* **11** 4831
[12] Giubileo F, Di Bartolomeo A, Iemmo L, Luongo G, Passacantando M, Koivusalo E, Hakkarainen T V and Guina M 2017 *Nanomaterials* **7** 275
[13] Stehr J E, Dobrovolsky A, Sukrittanon S, Kuang Y, Tu C W, Chen W M and Buyanova I A 2015 *Nano Lett.* **15** 242
[14] Dobrovolsky A, Stehr J E, Sukrittanon S, Kuang Y, Tu C W, Chen W M and Buyanova I A 2014 *Small* **11** 6331–7
[15] Buyanova I A and Chen W M 2019 *Nanotechnol.* **30** 292002
[16] Chen S, Jansson M, Stehr J E, Huang Y, Ishikawa F, Chen W M and Buyanova I A 2017 *Nano Lett.* **17** 1775
[17] Chen S, Yukimune M, Fujiwara R, Ishikawa F, Chen W M and Buyanova I A 2019 *Nano Lett.* **19** 885
[18] Weyers M and Sato M 1992 *Japan. J. Appl. Phys.* **31** 1853
[19] Kondow M, Uomi K, Hosomi K and Mozume T 1994 *Japan. J. Appl. Phys.* **33** L1056
[20] Bi W G and Tu C W 1997 *Appl. Phys. Lett.* **70** 1608
[21] Uesugi K, Marooka N and Suemune I 1999 *Appl. Phys. Lett.* **74** 1254
[22] Shan W, Walukiewicz W, Ager J, Haller E, Geisz J, Friedman D, Olson J and Kurtz S 1999 *Phys. Rev. Lett.* **82** 1221
[23] Ho I and Stringfellow G B 1997 *J. Cryst. Growth* **178** 1
[24] Zhang S B and Wei S H 2001 *Phys. Rev. Let.* **86** 1789
[25] Thinh N Q, Buyanova I A, Chen W M, Xin H P and Tu C W 2001 *Appl. Phys. Lett.* **79** 3089
[26] Li W, Pessa M, Ahlgren T and Decker J 2001 *Appl. Phys. Lett.* **79** 1094
[27] Toivonen J, Hakkarainen T, Sopanen M, Lipsanen H, Oila J and Saarinen K 2003 *Appl. Phys. Lett.* **82** 40
[28] Buyanova I A, Chen W M and Tu C W 2004 Defects in dilute nitrides *J. Phys.: Condens. Matter.* **16** S3027
[29] Wang X J, Puttisong Y, Tu C W, Ptak A J, Kalevich V K, Egorov A Y, Geelhaar L, Riechert H, Chen W M and Buyanova I A 2009 *Appl. Phys. Lett.* **95** 241904
[30] Buyanova I A, Chen W M, Monemar B, Xin H P and Tu C W 1999 *Appl. Phys. Lett.* **75** 3781
[31] Kondow M and Kitani T 2002 *Semicond. Sci. Technol.* **17** 746

[32] Bank S R, Yuen H B, Wistey M A, Lordi V, Bae H P and Harris J S Jr 2005 *Appl. Phys. Lett.* **87** 021908
[33] Fedorenko Y, Jouhti T, Pavelescu E-M, Karirinne S, Kontinnen J and Pessa M 2003 *Thin Solid Films* **440** 195
[34] Geelhaar L, Galluppi M, Jaschke G, Averbeck R, Riechert. H, Remmele T, Albrecht M, Dworzak M, Hildebrant R and Hoffmann A 2006 *Appl. Phys. Lett.* **88** 011903
[35] Kageyama T, Miyamoto T, Makino S, Koyama F and Iga K 1999 *Japan. J. Appl. Phys.* **38** L298
[36] Buyanova I A, Pozina G, Hai P N, Thinh N Q, Bergman J P, Chen W M, Xin H P and Tu C W 2000 *Appl. Phys. Lett.* **77** 2325
[37] Loke W K, Yoon S F, Wang S Z, Ng T K and Fan W J 2002 *J. Appl. Phys.* **91** 4900
[38] Yukimune M *et al* 2019 *Nanotechnology* **30** 244002
[39] Jahn U, Lahnemann J, Pfuller C, Brandt O, Breuer S, Jenichen B, Ramsteiner M, Geelhaar L and Riechert H 2012 *Phys. Rev.* B **85** 045323
[40] Heiss M *et al* 2011 *Phys. Rev.* B **83** 045303
[41] Spirkoska D *et al* 2009 *Phys. Rev.* B **80** 245325
[42] Graham A M, Corfdir P, Heiss M, Conesa-Boj S, Uccelli E, Fontcuberta i Morral A and Phillips R T 2013 *Phys. Rev.* B **87** 125304
[43] Pimenta A C S, Teles Ferreira D C, Roa D B, Moreira M V B, de Oliveira A G, Gonzalez J C, De Giorgi M, Sanvitto D and Matinaga F M 2016 *J. Phys. Chem.* C **120** 17046
[44] Bolinsson J, Ek M, Trägårdh J, Mergenthaler K, Jacobsson D, Pistol M-E, Samuelson L and Gustafsson A 2014 *Nano Res.* **7** 473
[45] Chen S L, Filippov S, Ishikawa F, Chen W M and Buyanova I A 2014 *Appl. Phys. Lett.* **105** 253106
[46] Chen W M 2000 *Thin Solid Films* **364** 45
[47] Stoll S and Schweiger A 2006 *J. Magn. Reson.* **178** 42
[48] Jia Y Q, von Bardeleben H J, Stievenard D and Delerue C 1992 *Phys. Rev.* B **45** 1645
[49] Stehr J E, Chen S L, Jansson M, Ishikawa F, Chen W M and Buyanova I A 2016 *Appl. Phys. Lett.* **109** 203103
[50] Vorona I P, Mchedlidze T, Dagnelund D, Buyanova I A, Chen W M and Köhler K 2006 *Phys. Rev.* B **73** 125204